ACS OMEGA

http://pubs.acs.org/journal/acsodf

Article

Superconducting Flexible Organic/Inorganic Hybrid Compound Adhesives

Hiroshi Takashima,* Yoshiyuki Yoshida, and Mitsuho Furuse

Cite This: *ACS Omega* 2022, 7, 47405−47410

Read Online

ACCESS | Metrics & More | Article Recommendations

ABSTRACT: Superconducting pastes have been successfully developed from superconducting particles using conventional methods, thereby opening up new avenues for the application of superconducting materials. These pastes are isotropic one-component heat-curable adhesives belonging to the class of organic/inorganic hybrid compounds. In this work, superconducting pastes prepared using Nb or NbN superconducting particles are applied to solid substrates through screen printing and then heat-cured under optimized conditions to form single-phase thick films. The resistivity of the Nb and NbN films becomes zero at 7.2 and 10.5 K, respectively, indicating that both these films are superconductive at cryogenic temperatures. A large free-standing film of length approximately 130 mm is successfully developed using the NbN paste. The free-standing film is flexible and exhibits superconductivity at 11 K. These results demonstrate, for the first time, that superconductivity, flexibility, adhesion, and ink properties can be simultaneously achieved in organic/inorganic hybrid compounds.

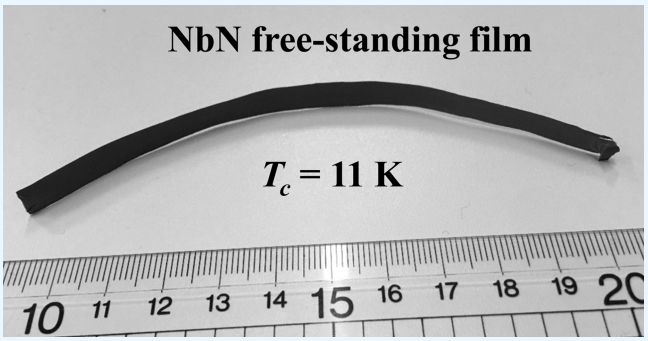

1. INTRODUCTION

Conductive pastes have been developed to fabricate circuit boards for electronic devices, electrodes for displays, and piezoelectric component flexible printed circuit boards. Conductive pastes, also known as isotropic one-component heat-curable conductive adhesives, and silver paste are types of organic/inorganic hybrid compounds.[1−9] Typically, heat curing is performed in air at 100−200 °C with a holding time of several tens of minutes. The paste can selectively achieve a wide range of viscosities, which is very important for ink materials used in screen printing and inkjet technologies. After thermal curing, the pastes exhibit excellent mechanical flexibility, electrical and mechanical connectivity, and handling properties. One application of such pastes is in printed circuit boards for integrated circuits in electronic devices,[10,11] where the superconducting state can be maintained at cryogenic temperatures to achieve wiring without power loss. Superconducting pastes can be applied as a fundamental component of superconducting joints of wires and thin films and in superconducting interconnects in multilayered devices.[12] Regarding the electrical conduction mechanism, it is generally believed that the hardening and shrinking of the binder cause the conductive fillers to come into contact with each other, resulting in electrical conduction. Therefore, to improve the conduction performance, the fillers should be as close to each other as possible, and a binder that has a large shrinkage rate and more filler contact points should be selected. Many studies have reported the preparation of filler particles, nanoparticles, and flakes.[2,3,6,8] If the factors that directly affect the conductivity and electrical conduction mechanism (e.g., curing conditions, binders, and solvents used as materials) can be clarified, new applications can be developed. This report describes the first prototype of paste preparation using Nb and NbN superconducting powders, which are well-known chemically stable superconductors. To optimize the solidification conditions, the shrinkage behavior and reaction during heat curing are studied in situ; the temperature dependence of resistivity is also investigated. A prototype free-standing film superconductor with mechanical flexibility is fabricated and studied as an application of this paste technology.

2. EXPERIMENTS, RESULTS, AND DISCUSSION

2.1. Nb Paste Preparation and Electrical Properties.

The synthesis method that is well known for the production of silver pastes was used to prepare the Nb conductive paste. First, Nb superconducting metal powder (purity ≥ 99.8%),

Received: October 29, 2022
Accepted: November 28, 2022
Published: December 7, 2022

https://doi.org/10.1021/acsomega.2c06977
ACS Omega 2022, 7, 47405−47410

epoxy resin (bisphenol A), solvent [diethylene glycol dibutyl ether (DGDB)], hardener (ammonium hexafluoroantimonate), and printing enhancer (silane coupling agent) were weighed. The weight ratios were as follows: Nb superconducting metal powder 80.0%, epoxy resin 8.0%, DGDB 11.0%, and hardener and printing enhancer 1.0%. The weighed materials were premixed using a planetary centrifugal mixer, and the resultant mixture was kneaded multiple times using a three-roll mill to prepare the final paste. Consequently, the superconducting powder, epoxy resin, curing agent, and printing enhancer were uniformly dispersed in the solvent.

Next, the paste was applied to a solid substrate through screen printing using a metal mask. The metal mask was made of a thin stainless steel plate with apertures for the printed structure. The paste was printed on a solid substrate through the metal mask using a plastic brush (squeegee). Therefore, the initial printing thickness was the thickness of the metal mask. As the printing structure was processed on the mask, the thickness of the printing film and structure could be freely selected, and the bonding area (volume) could be easily changed. After the paste was printed on the solid substrate, a solidification step was performed. In this study, a 6 mm × 6 mm structure was processed on the metal mask, and a $SrTiO_3(001)$ single crystal, which was commonly used as a substrate for $YBa_2Cu_3O_{7-\delta}$ thin films, was chosen as the solid substrate.

To optimize the solidification temperature of the paste, thermogravimetry−differential thermal analysis (TG−DTA) measurements, which can provide important information regarding thermal behavior,[13] were performed over the temperature range between room temperature and 500 °C. The TG results in Figure 1a show that weight loss begins at approximately 80 °C because of the vaporization of the DGDB. The DTA results indicate that vaporization of the epoxy and solvent begins at approximately 200 °C. The TG−DTA results show an exothermic reaction and weight loss at approximately 367 °C, corresponding to the thermal decomposition of the epoxy. The results also show heat generation and weight gain resulting from the Nb oxidation at approximately 475 °C. Because a slight change was observed in the DTA curve at approximately 145 °C, differential scanning calorimetry was performed for further investigation. An exothermic reaction corresponding to the curing reaction of epoxy was confirmed at 140−149 °C. Based on these results, the appropriate curing temperature was determined to be above 149 °C, which is sufficient for the epoxy to cure, and below 200 °C, at which the epoxy and solvent began to undergo exothermic processes. We decided on a curing temperature of 180 °C to ensure reproducibility. To precisely investigate the solidification process, the temperature and heat shrinkage of the paste were measured in situ. The temperature of the paste was measured using a radiation thermometer, and the position information in the direction of the height was measured with a laser using a resin cure shrinkage stress measuring device (Custron, AcroEdge Corporation). The results are shown in Figure 1b. The red color represents the sample temperature, and the purple color represents the shrinkage ratio. As the temperature increases, the paste monotonously shrinks because of the vaporization of the solvent, from approximately 50 °C. After heating at 180 °C for 20 min, the shrinkage almost saturates, and the final shrinkage ratio is approximately 24%. The results of the in situ shrinkage measurements indicate that

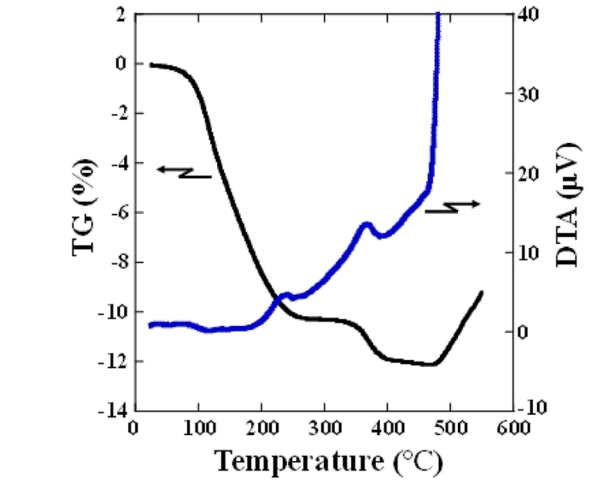

(a)

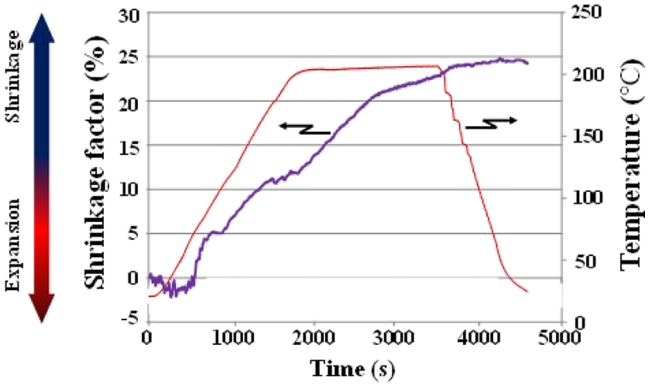

(b)

Figure 1. (a) TG−DTA curves of the Nb paste. The TG results show that weight loss begins at approximately 80 °C because of the vaporization of the DGDB. The DTA results indicate that vaporization of the epoxy and solvent begins at approximately 200 °C. The TG−DTA results show exothermic reactions and weight loss at approximately 367 °C, corresponding to the thermal decomposition of the epoxy. The heat generation and weight gain due to Nb oxidation at approximately 475 °C is also observed. (b) Measurement of heat shrinkage during solidification of the Nb paste. The temperature of the paste was measured with a radiation thermometer, and the position information in the height direction of the paste was measured with a laser. The sample temperature is indicated in red and the shrinkage ratio in purple. As the temperature increases, monotonous shrinkage is observed. This is because vaporization begins at approximately 50 °C in the solvent, the sample retention temperature is 200 °C for 20 min, and the shrinkage almost saturates in the atmosphere. Next, when the holding temperature is reduced, shrinkage occurs, although slightly. This is the result of the shrinkage due to the temperature drop. From these results, it is clear that the above-mentioned conditions of temperature and time are sufficient for solidification. The final shrinkage rate in this solidification process is approximately 24%.

a temperature of 180 °C and holding time of 20 min are optimal for solidification.

When printed and heat-cured under optimized conditions using a 200 μm-thick metal mask, the film thickness measured with a micrometer was 150 μm, indicating a reduction of approximately 25% in the thickness. This shrinkage is the result of densification due to solvent evaporation and is consistent with the shrinkage rate discussed above. The X-ray diffraction

https://doi.org/10.1021/acsomega.2c06977
ACS Omega 2022, 7, 47405−47410

(XRD) results are shown in Figure 2a. The (001) and (002) diffraction peaks of the $SrTiO_3$(001) single-crystal substrate

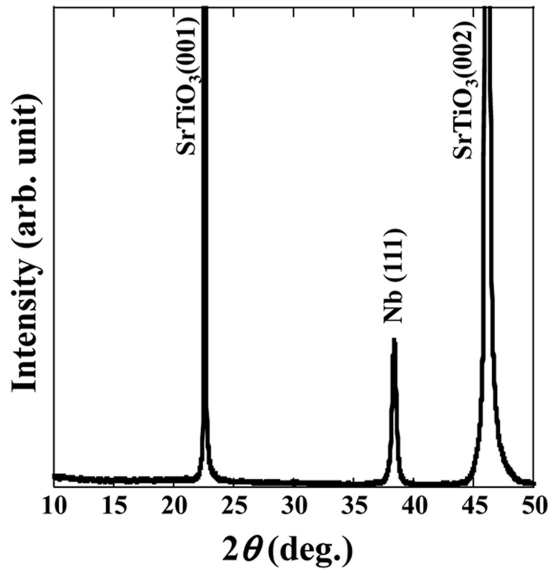

Figure 2. (a) XRD results of the Nb paste after solidification. The (001) and (002) diffraction peaks of the $SrTiO_3$(001) single-crystal substrate and the (111) diffraction peak of Nb are confirmed. There were no other impurity peaks. As a result, the paste is confirmed to be composed of Nb alone. (b) Cross-sectional SEM image of the paste after solidification. The Nb paste was solidified on a $SrTiO_3$(001) single-crystal substrate. Rectangular Nb fillers can be observed with a maximum of 60 μm among Nb particles with an average size of 10 μm. It can be seen that many fillers are in close contact with the adjacent fillers. This close contact is responsible for the electrical connections.

and the (111) diffraction peak of Nb can be confirmed. No other impurity peaks are observed. Consequently, it can be confirmed that the paste is composed of Nb alone. Figure 2b shows a cross-sectional scanning electron microscopy (SEM) image of the paste after solidification. The Nb paste is solidified on a $SrTiO_3$(001) single-crystal substrate. Rectangular Nb fillers with an average size of 10 μm can be observed, and the maximum dimension of the Nb particles is approximately 60 μm. It can be seen that many fillers are in close contact with the adjacent fillers, which is the reason for the electrical connections between neighboring particles.

To investigate the electrical properties of the solidified paste, three samples were prepared on a $SrTiO_3$(001) substrate using the screen-printing method. The thicknesses of the metal masks used were 100, 200, and 300 μm, respectively. After heat curing, the thicknesses of the pastes were 80, 150, and 230 μm, respectively. The resistivities of the samples were measured using a physical property measurement system (PPMS; Quantum Design), using the four-terminal method. The representative results are shown in Figure 3. It can be seen

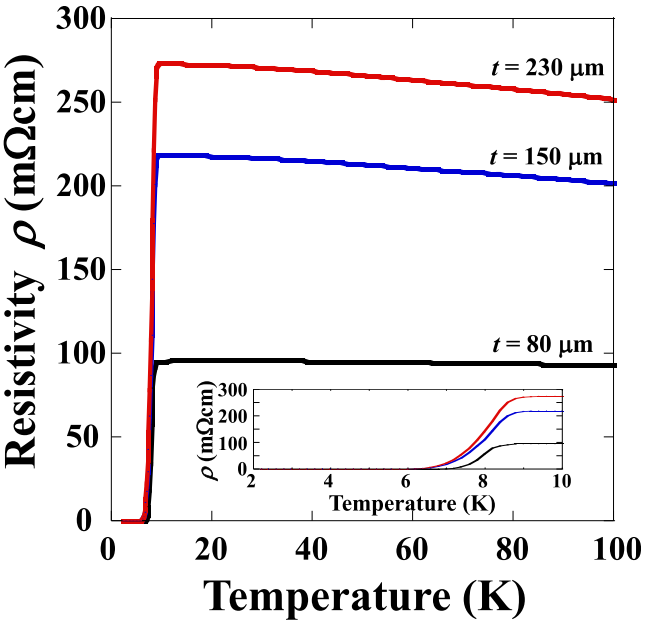

Figure 3. Temperature dependence of resistivity of the Nb paste after solidification. It can be seen that the samples show slightly greater resistivity from 100 K to lower temperatures, at 80, 150, and 230 μm thicknesses, as measured by a micrometer, after heat curing. A change in resistivity can be seen from approximately 8.2 to 9.0 K. The resistivity becomes zero from approximately 6.7 to 7.2 K, indicating superconductivity.

that, in the temperature range of approximately 10−100 K, the thicker the sample, the higher the resistivity. A sharp change in resistivity begins in the approximate range of 8.2−9.0 K. The resistivity becomes zero in the approximate range of 6.7−7.2 K, indicating that the paste has become a superconductor. According to previous reports,[14−16] the superconducting transition temperature (T_c) of bulk Nb and thin-film Nb was 9.2 and 8.2 K, respectively. The T_c of our superconducting paste was the same as that of the thin film, indicating that our superconducting paste was of high quality. In the thickness range from 80 to 230 μm, the thickness dependence of T_c was minimal.

To prepare a superconducting paste, it is important to use Nb powders containing particles of different sizes. Nb powders with average particle sizes of 10 and 45 μm were used in the above samples. When the paste was made with only the respective particles (10 and 45 μm), superconductivity was not observed at temperatures above 4.2 K. When only small particles were used, the lack of superconductivity above 4.2 K could be attributed to the degradation of the superconductivity of the Nb particles in the paste. When only large particles were used, it was difficult to prepare a paste with sufficient viscosity for printing when the Nb particle content was ≥60%. When a paste was prepared by mixing the particles, superconducting

https://doi.org/10.1021/acsomega.2c06977
ACS Omega 2022, 7, 47405−47410

transition was confirmed at temperatures above 4.2 K. To achieve the highest transition temperature, the weight ratio of the 10 to 45 μm particles was 7:3. The superconductivity is the result of the electrical conduction caused by the contact between Nb superconducting particles of two sizes because of the curing shrinkage of the binder during heat curing at 180 °C for 20 min.

2.2. NbN Paste Preparation and Electrical Properties. The preparation method for the NbN conductive paste was the same as that for the Nb conductive paste. NbN superconducting metal powder (purity ≥ 98%), epoxy resin (bisphenol A), solvent (DGDB), hardener (ammonium hexafluoroantimonate), and printing enhancer (silane coupling agent) were weighed. The weight ratios were as follows: NbN superconducting metal powder 80.0%, epoxy resin 8.0%, DGDB 11.0%, and hardener and printing enhancer 1.0%. The weighed materials were premixed using a planetary centrifugal mixer, and the resultant mixture was kneaded multiple times using a three-roll mill to prepare the final paste. Consequently, the superconducting powder, epoxy resin, curing agent, and printing enhancer were uniformly dispersed in the solvent.

Next, the paste was applied to $SrTiO_3(001)$ single-crystal substrates by the screen-printing method using various metal masks of thicknesses 100, 200, 300, and 400 μm. After heat curing, the thicknesses of the pastes were 80, 150, 220, and 300 μm, respectively. The results indicate that the shrinkage ratio of the NbN paste is similar to that of the Nb paste. The XRD results are shown in Figure 4a. The (001) and (002) diffraction peaks of the $SrTiO_3(001)$ single-crystal substrate and that of NbN are confirmed. No other impurity peaks are observed. Therefore, it can be confirmed that the paste is composed of NbN alone. Figure 4b shows a cross-sectional SEM image of the paste after solidification. It is found that the NbN paste solidifies on the $SrTiO_3(001)$ single-crystal substrate. It can be seen that cuboidal NbN fillers are closely packed and that many fillers are in contact with the adjacent fillers.

The electrical properties of the pastes solidified on the $SrTiO_3(001)$ substrates were investigated using PPMS through a four-terminal method (Figure 5). It can be seen that all the samples show metallic electrical conductivity from 100 to approximately 20 K, and a sharp drop can be seen at approximately 16 K. The resistivity becomes zero at approximately 10.5 K, indicating that the pastes become superconductors. According to previous reports,[14,17−20] the T_c of both bulk and thin-film NbN is 16 K. Our superconducting paste had a slightly lower T_c than the bulk and thin-film NbN. The dependence of T_c on the film thickness was almost negligible in the thickness range of 80−300 μm.

2.3. Preparation and Electrical Properties of Free-Standing Films. Free-standing films without solid substrates are very useful for achieving flexibility, selective formability, and large-scale applicability.[21−25] To demonstrate the flexibility and formability, a free-standing superconductor film was prepared as a new application of our proposed paste technology. The free-standing films were prepared by the method described above using NbN paste with a high T_c. A thin flexible stainless-steel sheet was used as the solid substrate. A stainless-steel plate with a thickness of 400 μm with a 6 mm × 140 mm structure fabricated on it was used as the metal mask.

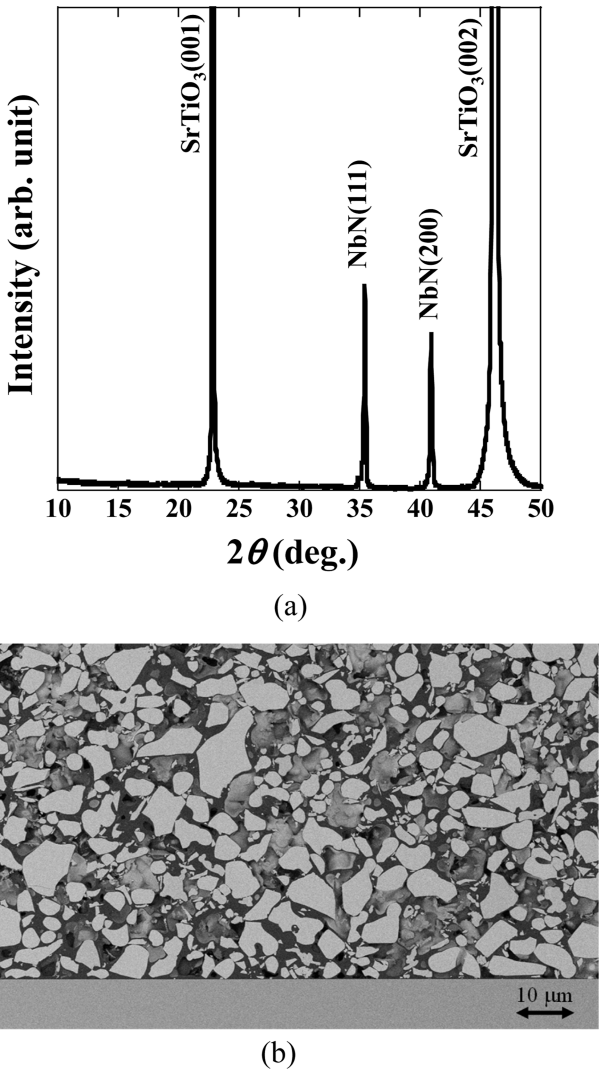

Figure 4. (a) XRD result of the NbN paste after solidification. The (001) and (002) diffraction peaks of the $SrTiO_3(001)$ single-crystal substrate and the diffraction peak of NbN are confirmed. There were no other impurity peaks. As a result, the paste is confirmed to be composed of NbN alone. (b) Cross-sectional SEM image of the paste after solidification. It is found that the NbN paste is solidified on the $SrTiO_3(001)$ single-crystal substrate, and the film thickness is approximately 80 μm. A cuboidal NbN filler can be confirmed with a maximum size of 30 μm. It can be seen that many fillers are in contact with the adjacent fillers.

Once completely solidified, it is very difficult to peel the film off from the stainless-steel plate; therefore, a two-step heat-curing process was used to prepare the free-standing film. First, the paste was applied to the solid substrate by screen printing using a metal mask. After printing, the paste was placed in a drying oven at 180 °C for 5 min to temporarily solidify in air. As a result, some of the DGDB used as the solvent evaporated, and the paste became semi-raw. Next, the thin stainless steel sheet solid substrate and semi-raw printed sheet were carefully peeled off to form a free-standing film. Then, the free-standing film was dried at 180 °C for 20 min to evaporate the DGDB and cause a curing reaction of the epoxy resin. Figure 6a(1) shows a photograph of the prepared free-standing NbN film. It was 5 mm wide and 130 mm long with a thickness of 300 μm. Figure 6a(2) shows that the two ends of the film can be connected to create a ring, demonstrating that the film is

https://doi.org/10.1021/acsomega.2c06977
ACS Omega 2022, 7, 47405−47410

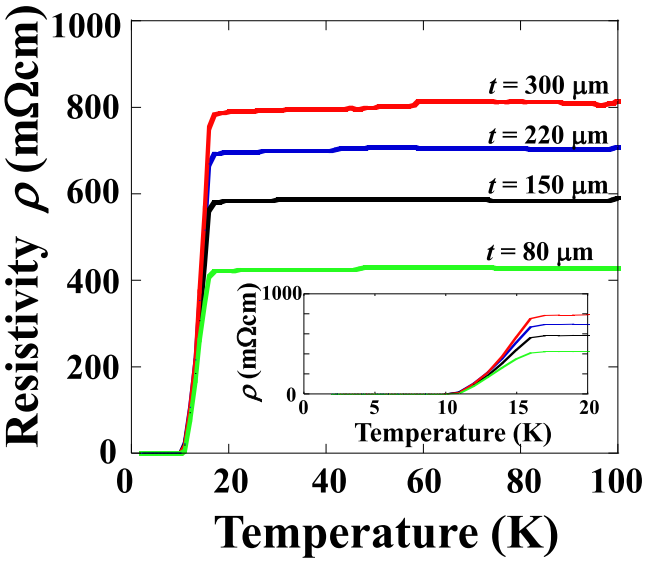

Figure 5. Temperature dependence of resistivity of the NbN paste after solidification. It can be seen that the paste after solidification shows metallic electrical conductivity from 100 K to low temperatures, at 80, 150, 220, and 300 μm thicknesses, as measured by a micrometer, after heat curing. A change in resistivity can be seen at approximately 16 K. The resistivity becomes zero at approximately 10.5 K, indicating superconductivity.

flexible. The temperature dependence of the resistivity of the free-standing film was investigated at several points on the film using a PPMS following the four-terminal method. The results are shown in Figure 6b. It can be seen that the sample shows metallic electrical conductivity from 100 to just below 20 K, and a sharp drop in resistivity begins at approximately 15 K. The resistivity becomes zero at approximately 11 K, indicating that the free-standing film becomes a superconductor below this temperature. The superconductivity is the result of the electrical conduction caused by the contact between the NbN superconducting particles owing to the curing shrinkage of the binder during heat curing at 180 °C for 20 min.

These results are fundamental for producing printed circuit board wiring for superconducting devices that require integration and use the screen-printing method. The proposed technology is also fundamental for fabricating flexible superconducting free-standing films. This technology is expected to be useful for creating superconducting connections[12,25−27] that maintain both superconductivity and mechanical links between wires and thin films and for superconducting interconnect technology in multilayered devices that electrically and mechanically connect the upper and lower layers,[28−30] which can act as adhesives with superconducting properties.

3. CONCLUSIONS

We developed a superconducting paste, which was an isotropic one-component heat-curable adhesive of the organic/inorganic hybrid compound type, opening up a new avenue for superconducting material applications. The superconducting paste prepared by the conventional method using Nb or NbN particles was applied to solid substrates by screen printing and heat-cured under optimized conditions. It was found that, after solidification, the thick films had a single phase without impurities. The resistivities of the Nb and NbN films became zero at 7.2 and 10.5 K, respectively, indicating superconductivity. A large free-standing NbN film with length

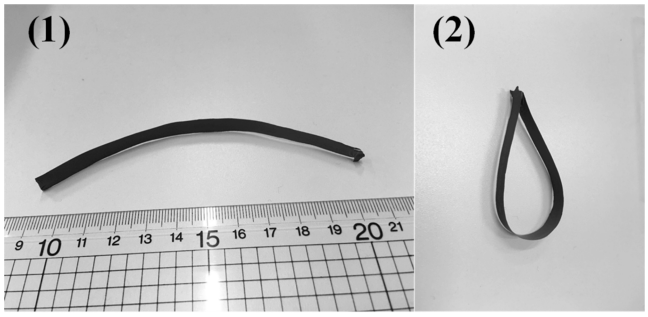

(a)

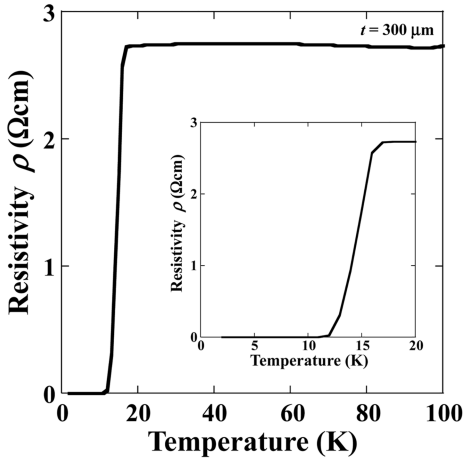

(b)

Figure 6. (a) Photograph of the prepared free-standing NbN film. (1) It is 5 mm wide and 130 mm long, with a thickness of 300 μm. (2) The two ends are connected to create a ring, which is flexible. (b) Temperature dependence of resistivity of the free-standing NbN film. It can be seen that the paste after solidification shows metallic electrical conductivity from 100 K to low temperatures at 300 μm thickness and that a change in resistivity begins at approximately 15 K. The resistivity becomes zero at approximately 11 K, indicating superconductivity.

greater than 10 cm was successfully developed. The resistivity of the free-standing film became zero at 11 K, indicating that it became a superconductor at this temperature. This was a result of the electrical conduction caused by the contact between the NbN superconducting particles owing to curing shrinkage of the binder during heat curing at 180 °C for 20 min. The close contact of many fillers with neighboring fillers caused electrical connections between the superconducting particles, resulting in superconductivity. These results demonstrate, for the first time, the simultaneous achievement of superconductivity, flexibility, adhesion, and ink properties in organic/inorganic hybrid. This technology is appropriate for screen-printed circuit board wiring of superconducting devices that may require integration in the future and is also expected to be useful for creating superconducting connections that maintain superconductivity and mechanical links between wires and thin films.

https://doi.org/10.1021/acsomega.2c06977
ACS Omega 2022, 7, 47405−47410

AUTHOR INFORMATION

Corresponding Author

Hiroshi Takashima − *Research Institute for Advanced Electronics and Photonics, National Institute of Advanced Industrial Science and Technology, Tsukuba, Ibaraki 305-8568, Japan;* orcid.org/0000-0002-3437-468X; Phone: +81-29-861-5594; Email: h-takashima@aist.go.jp; Fax: +81-29-861-5387

Authors

Yoshiyuki Yoshida − *Research Institute for Advanced Electronics and Photonics, National Institute of Advanced Industrial Science and Technology, Tsukuba, Ibaraki 305-8568, Japan*

Mitsuho Furuse − *Research Institute for Energy Conservation, National Institute of Advanced Industrial Science and Technology, Tsukuba, Ibaraki 305-8568, Japan*

Complete contact information is available at: https://pubs.acs.org/10.1021/acsomega.2c06977

Notes

The authors declare no competing financial interest.

ACKNOWLEDGMENTS

This paper is based on the results obtained from a project commissioned by the New Energy and Industrial Technology Development Organization (NEDO).

REFERENCES

(1) Li, Z.; Zhang, R.; Moon, K.-S.; Liu, Y.; Hansen, K.; Le, T.; Wong, C. P. Highly Conductive, Flexible, Polyurethane-Based Adhesives for Flexible and Printed Electronics. *Adv. Funct. Mater.* **2013**, *23*, 1459−1465.

(2) Kamyshny, A.; Magdassi, S. Conductive Nanomaterials for Printed Electronics. *Small* **2014**, *10*, 3515−3535.

(3) Jiang, H.; Moon, K.-S.; Li, Y.; Wong, C. P. Surface Functionalized Silver Nanoparticles for Ultrahigh Conductive Polymer Composites. *Chem. Mater.* **2006**, *18*, 2969−2973.

(4) Nguyen, H.-V.; Andreassen, E.; Kristiansen, H.; Johannessen, R.; Hoivik, N.; Aasmundtveit, K. E. Rheological characterization of a novel isotropic conductive adhesive − Epoxy filled with metal-coated polymer spheres. *Mater. Des.* **2013**, *46*, 784−793.

(5) Tsurumi, N.; Tsuji, Y.; Baba, T.; Murata, H.; Masago, N.; Yoshizawa, K. Comparative study of the ideal and actual adhesion interfaces of the die bonding structure using conductive adhesives. *J. Adhes.* **2022**, *98*, 24−48.

(6) Chen, S.; Mei, Y.-H.; Wang, M.; Li, X.; Lu, G.-Q. Large-Area Bonding by Sintering of a Resin-Free Nanosilver Paste at Ultralow Temperature of 180 °C. *IEEE Trans. Compon., Packag., Manuf. Technol.* **2022**, *12*, 707−710.

(7) Si, P.; Trinidad, J.; Chen, L.; Lee, B.; Chen, A.; Persic, J.; Lyn, R.; Leonenko, Z.; Zhao, B. PEDOT:PSS nano-gels for highly electrically conductive silver/epoxy composite adhesives. *J. Mater. Sci.: Mater. Electron.* **2018**, *29*, 1837−1846.

(8) Zhang, Z. X.; Chen, X. Y.; Xiao, F. The Sintering Behavior of Electrically Conductive Adhesives Filled with Surface Modified Silver Nanowires. *J. Adhes. Sci. Technol.* **2012**, *25*, 1465−1480.

(9) Hyun, W. J.; Lim, S.; Ahn, B. Y.; Lewis, J. A.; Frisbie, C. D.; Francis, L. F. Screen Printing of Highly Loaded Silver Inks on Plastic Substrates Using Silicon Stencils. *ACS Appl. Mater. Interfaces* **2015**, *7*, 12619−12624.

(10) Brusic, V.; Frankel, G. S.; Roldan, J.; Saraf, R. Corrosion and Protection of a Conductive Silver Paste. *J. Electrochem. Soc.* **1995**, *142*, 2591−2594.

(11) Fang, J.; Fu, R.; Zou, Y.; Liu, H.; Liu, X. Hybrid silver pastes with synergistic effect of multi-scale silver fillers and the application in flexible circuits. *Mater. Res. Express* **2021**, *8*, 096303.

(12) Brittles, G. D.; Mousavi, T.; Grovenor, C. R. M.; Aksoy, C.; Speller, S. C. Persistent current joints between technological superconductors. *Supercond. Sci. Technol.* **2015**, *28*, 093001.

(13) Lu, C.-A.; Lin, P.; Lin, H.-C.; Wang, S.-F. Effects of Silver Oxide Addition on the Electrical Resistivity and Microstructure of Low-Temperature-Curing Metallo-Organic Decomposition Silver Pastes. *Jpn. J. Appl. Phys.* **2007**, *46*, 4179−4183.

(14) Matthias, B. T.; Geballe, T. H.; Compton, V. B. Superconductivity. *Rev. Mod. Phys.* **1963**, *35*, 1−22.

(15) McMillan, W. L. Transition Temperature of Strong-Coupled Superconductors. *Phys. Rev.* **1968**, *167*, 331−344.

(16) Shimizu, Y.; Tonooka, K.; Yoshida, Y.; Furuse, M.; Takashima, H. Room-temperature growth of thin films of niobium on strontium titanate (0 0 1) single-crystal substrates for superconducting joints. *Appl. Surf. Sci.* **2018**, *444*, 71−74.

(17) Aschermann, G.; Friderich, E.; Justi, E.; Kramer, J. Supraleitfähige Verbindungen mit extrem hohen Sprungtemperaturen (NbH und NbN). *Phys. Z* **1941**, *42*, 349−360.

(18) Haley, F. C.; Andrews, D. H. An Anomalous Critical Current Effect in Superconducting NbN. *Phys. Rev.* **1953**, *89*, 821−823.

(19) Shinoki, F.; Takada, S.; Kosaka, S.; Hayakawa, H. Fabrication of High Quality NbN/Pb Josephson Junction. *Jpn. J. Appl. Phys.* **1980**, *19*, 591−594.

(20) Shoji, A.; Shinoki, F.; Kosaka, S.; Aoyagi, M.; Hayakawa, H. New fabrication process for Josephson tunnel junctions with (niobium nitride, niobium) double-layered electrodes. *Appl. Phys. Lett.* **1982**, *41*, 1097.

(21) Vendamme, R.; Onoue, S.; Nakao, A.; Kunitake, T. Robust free-standing nanomembranes of organic/inorganic interpenetrating networks. *Nat. Mater.* **2006**, *5*, 494−501.

(22) Cong, H.-P.; Ren, X.-C.; Wang, P.; Yu, S.-H. Flexible graphene−polyaniline composite paper for high-performance supercapacitor. *Energy Environ. Sci.* **2013**, *6*, 1185−1191.

(23) Liu, F.; Seo, T. S. A Controllable Self-Assembly Method for Large-Scale Synthesis of Graphene Sponges and Free-Standing Graphene Films. *Adv. Funct. Mater.* **2010**, *20*, 1930−1936.

(24) Menard, E.; Nuzzo, R. G.; Rogers, J. A. Bendable single crystal silicon thin film transistors formed by printing on plastic substrates. *Appl. Phys. Lett.* **2005**, *86*, 093507.

(25) Saraswat, G.; Gupta, P.; Bhattacharya, A.; Raychaudhuri, P. Highly oriented, free-standing, superconducting NbN films growth on chemical vapor deposited graphene. *APL Mater.* **2014**, *2*, 056103.

(26) Ohki, K.; Nagaishi, T.; Kato, T.; Yokoe, D.; Hirayama, T.; Ikuhara, Y.; Ueno, T.; Yamagishi, K.; Takao, T.; Piao, R.; Maeda, H.; Yanagisawa, Y. Fabrication, microstructure and persistent current measurement of an intermediate grown superconducting (iGS) joint between REBCO-coated conductors. *Supercond. Sci. Technol.* **2017**, *30*, 115017.

(27) Matsumoto, R.; Iwata, H.; Yamashita, A.; Hara, H.; Nishijima, G.; Tanaka, M.; Takeya, H.; Takano, Y. Superconducting joints using Bi-added PbSn solders. *Appl. Phys. Express* **2017**, *10*, 093102.

(28) Wellstood, F. C.; Kingston, J. J.; Clarke, J. Thin-film multilayer interconnect technology for $YBa_2Cu_3O_{7-x}$. *J. Appl. Phys.* **1994**, *75*, 683−702.

(29) Takashima, H.; Kasai, N.; Shoji, A. Fabrication of grain boundary Josephson junction on top layer of YBCO multilayer using chemical mechanical planarization. *Phys. C* **2003**, *392−396*, 1367−1372.

(30) Takashima, H.; Kasai, N.; Shoji, A. Fabrication of High-Quality $YBa_2Cu_3O_{7-\delta}$ Multilayer Structure Using Chemical Mechanical Planarization for Superconducting Quantum Interference Device Gradiometer. *Jpn. J. Appl. Phys.* **2002**, *41*, L1062.